electronic reprint

STRUCTURAL SCIENCE
CRYSTAL ENGINEERING
MATERIALS

ISSN: 2052-5206
journals.iucr.org/b

Synthesis, structure and non-linear optical properties of new isostructural β-D-fructopyranose alkaline halide metal–organic frameworks: a theoretical and an experimental study

Domenica Marabello, Paola Antoniotti, Paola Benzi, Carlo Canepa, Leonardo Mortati and Maria Paola Sassi

Acta Cryst. (2017). B**73**, 737–743

Acta Cryst B
STRUCTURAL SCIENCE
CRYSTAL ENGINEERING
MATERIALS
ISSN 2052-5206

Synthesis, structure and non-linear optical properties of new isostructural β-D-fructopyranose alkaline halide metal–organic frameworks: a theoretical and an experimental study

Domenica Marabello,[a,b]* Paola Antoniotti,[a,b] Paola Benzi,[a,b] Carlo Canepa,[a] Leonardo Mortati[c] and Maria Paola Sassi[c]

[a]Dipartimento di Chimica, Universitá degli Studi di Torino, Via P. Giuria 7, 10125 Torino, Italy, [b]CrisDi-Interdepartmental Center for Crystallography, University of Torino, Torino, Italy, and [c]INRIM – Istituto Nazionale di Ricerca Metrologica, Torino, Italy. *Correspondence e-mail: domenica.marabello@unito.it

Received 21 December 2016
Accepted 7 April 2017

Edited by P. Metrangolo, Politecnico di Milano, Italy

Keywords: metal–organic frameworks (MOFs); isomorphic material; non-linear optical properties; second-harmonic generating efficiency; structure–property relationship.

CCDC references: 1511464; 1511467

Supporting information: this article has supporting information at journals.iucr.org/b

In this work four metal–organic framework isomorphs, based on fructose and alkali-earth halogenides, were investigated to better understand the effect of the size of the cation and the different polarizability of the anion on the calculated hyperpolarizability and optical susceptibility, which are correlated to non-linear optical properties. The compounds were characterized by X-ray diffraction and the first hyperpolarizability and the second-order susceptibility were obtained from theoretical calculations. Furthermore, a new method to measure the second-harmonic (SH) efficiency on a small quantity of powder at different wavelengths of excitation was optimized and an attempt was made to assess the reduction of the SH intensity for small quantities of nano-crystals, in order to ascertain the possibility of applications in biological systems. The results of this work show that both the intrinsic nature of the anion and the induced dissociation of cations and anions by fructose play a role in the second-harmonic generating properties of such compounds.

1. Introduction

Non-linear optical (NLO) materials are required for multiple applications in laser technology, optical communication and data storage technology (Agullo-Lopez *et al.*, 1994). Moreover, second-harmonic generating (SHG) materials can be used in biology and medicine for microscopic *in vivo* imaging techniques (Pantazis *et al.*, 2010; Dempsey *et al.*, 2012; McKinlay *et al.*, 2010). Inorganic materials are widely used in these applications, but the optical linearity of these materials is not satisfying in terms of SHG efficiency with respect to organic compounds that can exhibit SHG efficiencies a thousand times those of inorganic NLO materials (Tam *et al.*, 1989). However, the organic NLO crystals are often difficult to grow, too fragile and also sometimes too chemically unstable for applications. In the last decades, some semi-organic materials combining the NLO properties of organic molecules with the stability of inorganic salts were considered for NLO applications. For example, among metal–organic coordination compounds several complexes of amino acids with inorganic salts have been surveyed (Jiang & Fang, 1999; Kuppler *et al.*, 2009; Chandrasekaran *et al.*, 2012; Dhanuskodi *et al.*, 2007). In particular, Jiang *et al.* showed that a combination of inorganic and organic materials provides a potentially useful approach to more efficient and more stable NLO crystals, providing the advantages of both an enhancement of the physico-chemical stability and an increase in NLO intensity *via* the metal–ligand

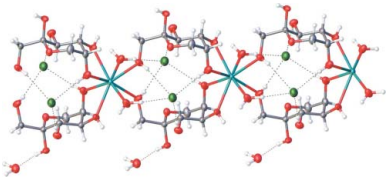

bridging interactions. In fact, both the central metal ion and the halogen anions have been proved to be involved in the promotion of the SHG efficiency.

NLO materials require the lack of an inversion centre in the crystal structure; to fulfill this requirement in semi-organic materials, chiral organic ligands can be utilized because pure inorganic salts more easily crystallize in centrosymmetric space groups. The presence of the asymmetric ligand drives the crystallization toward a new non-centrosymmetric material and makes it a good candidate for the NLO properties. One difficulty in the synthesis of chiral organic ligands is the separation of the two enantiomers. For this reason in this work we considered carbohydrate ligands, naturally synthesized in only one enantiomer, and also suitable asymmetric polydentate ligands that are able to coordinate alkali earth metals with the formation of metal–organic frameworks (MOFs). The SHG efficiency of many mono-, di- and trisaccharides has been examined, and a correlation between their crystal systems and SHG efficiencies has been shown, *i.e.* the lower the space-group symmetry of the crystal the larger its SHG efficiency (Bourhill *et al.*, 1993). In this work, we also focused our attention on complexes of saccharide and inorganic salts because of their non-toxic and bio-compatible properties, required for biological applications. Among inorganic salts, calcium and strontium compounds were considered, because these two metals are involved a variety of biological processes playing important physiological roles (*e.g.* calcium storage, bone calcification and calcium-dependent interactions in cells) and consequently showing large biocompatibility (Kannan *et al.*, 2010). Fructose was chosen as a carbohydrate ligand because of its large affinity toward alkaline-earth metals, its commercial availability and low cost.

In our previous work (Marabello *et al.*, 2015), we reported a theoretical and experimental study on the NLO properties of two MOFs obtained from fructose and calcium chloride, $[Ca(C_6H_{12}O_6)_2(H_2O)_2]Cl_2{\cdot}H_2O$ (CaFruCl) and $[Ca(C_6H_{12}O_6)(H_2O)_2]Cl_2$ (CaFruCl-2). We measured (Mortati *et al.*, 2012) their SH intensity by SHG microscopy and showed that the coordination of fructose on the calcium ion improves the SH efficiency with respect to fructose itself, probably by both the induced lowering of symmetry and the dissociation of $CaCl_2$. In this work we extended our investigation on MOFs obtained from fructose and other alkali-earth halogenides to better understand the effect of the size of the cation and the different polarizability of the anion in isomorphic structures on the calculated hyperpolarizability and optical susceptibility, which in turn are related to the SHG efficiency. In particular, we synthesized more isomorphs of CaFruCl of the formula $[M(C_6H_{12}O_6)_2(H_2O)_2]X_2{\cdot}H_2O$, with M = Ca, Sr and X = Cl, Br. Few complexes of fructose and inorganic salts are known in the literature (Craig *et al.*, 1974*a*,*b*; Cook & Bugg, 1976; Guo & Zhang, 2004), and for all of these the synthesis methodology implies the very slow evaporation of aqueous solutions with procedures that completed over several months. In this work, instead we optimized a new simple, rapid and low-cost synthesis methodology, free of any environmental impact. The compounds were characterized by X-ray diffraction and the resulting coordinates of the crystal fragments were used both to optimize, at the B3LYP level of theory, the geometries of the complexes and to calculate first hyperpolarizability (β) and second-order susceptibility [$\chi^{(2)}$]. As these compounds share the same crystalline structure, they represent an interesting opportunity to investigate how the SHG properties change with the nature of the cation and the anion. Furthermore, as most biological applications of NLO materials in recent years involve powdered samples (Haber *et al.*, 2011; Wunderlich & Peschel, 2013; Bäumner *et al.*, 2010; Staedler *et al.*, 2012), we also optimized a new method to measure the SHG efficiency on a small quantity of powder at different wavelengths of excitation, trying to determine the quadratic coefficient relevant to the second-order susceptibility. Furthermore, we also attempted to assess the reduction of the SH intensity for small quantities of nano-crystals, in order to ascertain the possibility of applications in biological systems.

2. Experimental

2.1. Synthesis of $[Ca(C_6H_{12}O_6)_2(H_2O)_2]Cl_2{\cdot}H_2O$ (CaFruCl)

The synthesis and X-ray structure determination of this compound are reported in our previous work (Marabello *et al.*, 2015).

2.2. Synthesis of $[Ca(C_6H_{12}O_6)_2(H_2O)_2]Br_2{\cdot}H_2O$ (CaFruBr)

Calcium bromide and β-D-fructose were ground together in an agate mortar at the stoichiometric ratio 1:2 and subsequently partially dissolved in a small amount of ethanol at room temperature. The solution at equilibrium with its solid was closed into a vial and numerous crystals of the compound were deposited on the walls of the vial after a few days. These crystals were filtered on paper and quickly dried under air flux at room temperature. The X-ray crystal structure of this compound was determined by Cook & Bugg (1976) but because the X-ray characterization was very old the X-ray structure of this compound was re-determined in order to obtain more accurate data for comparison with the compounds investigated in this work.

2.3. Synthesis of $[Sr(C_6H_{12}O_6)_2(H_2O)_2]Cl_2{\cdot}H_2O$ (SrFruCl)

Anhydrous calcium chloride and β-D-fructose were dissolved in ethanol at 348 K in the stoichiometric ratio 1:2. During the dissolution of the reagents a faint precipitate is deposited at the bottom of the solution. The solution was filtered and slowly evaporated at room temperature in a glass test-tube. After a few days a crystalline powder was deposited on the wall of the test-tube. These crystals were filtered on paper and quickly dried under air flux at room temperature. The X-ray crystal structure of this compound was determined by Guo & Zhang (2004) and for this work data deposited in the Cambridge Structural Database (CSD; CCDC reference 220667) were utilized.

Table 1
Cell parameters for compounds CaFruCl, CaFruBr, SrFruCl and SrFruBr.

All compounds in monoclinic space group $C2$ with $Z = 4$.

Compound	CaFruCl	CaFruBr	SrFruCl	SrFruBr
a (Å)	16.016 (1)	16.1449 (7)	16.252 (5)	16.439 (1)
b (Å)	7.8393 (2)	7.8881 (3)	7.941 (2)	8.0240 (5)
c (Å)	10.8679 (9)	11.4702 (5)	10.751 (3)	11.1931 (8)
β (°)	127.82 (1)	128.842 (4)	127.652 (4)	128.142 (7)
V (Å^3)	1077.9 (2)	1137.8 (1)	1098.5 (5)	1161.2 (2)

2.4. Synthesis of $[Sr(C_6H_{12}O_6)_2(H_2O)_2]Br_2{\cdot}H_2O$ (SrFruBr)

Calcium bromide and β-D-fructose were completely dissolved in ethanol at 348 K in the stoichiometric ratio 1:2. The solution was slowly evaporated at room temperature in a glass test-tube and after few days a crystalline powder was deposited on the wall of the test-tube. These crystals were filtered on paper and quickly dried under air flux at room temperature.

2.5. X-ray diffraction

X-ray diffraction data for compounds CaFruBr and SrFruBr were collected at room temperature using an Oxford Diffraction Gemini R Ultra diffractometer. Data were collected with graphite-monochromated Mo $K\alpha$ radiation (0.71073 Å). The *CrysAlisPro* (Agilent, 2014) package was used for data collection and integration, *SHELXT* (Sheldrick, 2015*a*) for resolution, *SHELXL* (Sheldrick, 2015*b*) for refinement and *Olex*2 (Dolomanov *et al.*, 2009) for graphics.

Both compounds crystallize in the monoclinic $C2$ space group with $Z = 2$. All but the H atoms were anisotropically refined. All H atoms were located on difference Fourier maps, but they were calculated and refined riding with $U_{iso} = 1.2$ or 1.5 U_{eq} of the bonded atom. CaFruBr: 7940 reflections measured, 3298 unique ($R_{int} = 0.0364$), $R1(F^2) = 0.0335$, $wR(F^2) = 0.0716$, max/min peak = 0.35/−0.56, CCDC 1511464. SrFruBr: 11 419 reflections measured, 5390 unique ($R_{int} = 0.0438$), $R1(F^2) = 0.0497$, $wR(F^2) = 0.0805$, max/min peak = 0.51/−0.89, CCDC 1511467.

Details of crystal data for all compounds are reported in Table 1.

2.6. Powder characterization

XRPD patterns of all samples were collected at room temperature using an Oxford Diffraction Gemini R Ultra diffractometer. Data were collected with mirror-monochromated Cu $K\alpha$ radiation ($\lambda = 1.5418$ Å): maximum resolution 1.4 Å, exposure time 30 s and data integration with *CrysAlisPro* software. Fourier transform (FT)–IR and FT–Raman spectra were collected using the Bruker Vertex 70 FT–IR spectrophotometer with the RAM II accessory, equipped with NdYAG laser (1064 nm) operating at 90 mW. The spectral resolution was 2 cm^{-1}.

The measurements were made directly on the samples. The XRPD patterns and IR and Raman spectra are reported in the supporting information.

2.7. Computational methods

The calculations were performed with the *GAUSSIAN*09 set of programs (Frisch *et al.*, 2009). All the structures in this work were optimized by gradient-based techniques (Schlegel & Daudel, 1981; Schlegel, 1982*a*,*b*; Schlegel *et al.*, 1984) without symmetry constraints at the DFT B3LYP (Becke, 1988, 1993) level of theory, in conjunction with the 6-31G(d) basis set (Hehre *et al.*, 1986). All critical points were characterized as energy minima, by analytical calculation of vibrational frequencies. The total dipole moments, polarizabilities and first-order hyperpolarizabilities were calculated at the same level of theory. Molecular volumes were computed by averaging ten different volume calculations on the optimized geometries at the B3LYP/6-31G(d) level of theory with the *GAUSSIAN*09 options scf=tight, volume=tight and iop(6/45=500,6/46=1) (Parsons & Ninham, 2009).

2.8. Second-harmonic generation spectral measurements

All compounds were characterized in terms of second-harmonic generation emission using an NLO multimodal microscope as described previously (Mortati *et al.*, 2012). The powdered compounds, with each individual crystal in a random orientation, were analyzed acquiring average images at different excitation wavelengths and powers, keeping the detector setting parameters (*i.e.* PMT voltage, gain and offset) fixed for all the measurements.

The measurements were repeated and averaged five times. Each image was processed by computing the average intensity related to the actual sample surface obtained by masking the image through an Otsu's threshold binary mask, avoiding the background contribution. The computed averages were quadratically fitted with the actual sample excitation powers excluding all the outliers to improve the curve fitting, using a method described in a previous work (Marabello *et al.*, 2015). In this work, the quadratic coefficients were extracted for different excitation wavelengths in a spectral range between

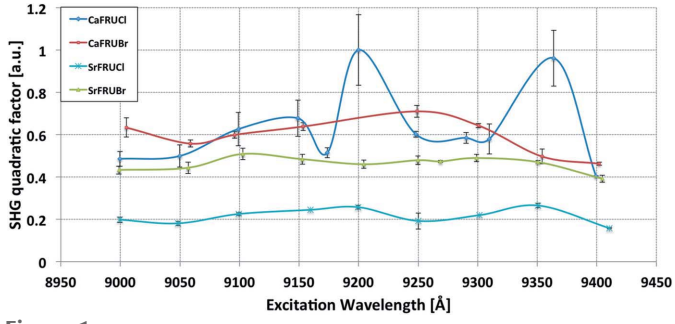

Figure 1
Quadratic fitting parameters (arbitrary units) of the SH intensities plotted as a function of the excitation power at different excitation wavelengths for all the analyzed compounds. Error bars represent the standard deviations around the average point computed from the extracted quadratic fitting parameters.

Table 2
Relevant distances (Å) around the metal atom from X-ray data and B3LYP/6-31G(d) calculations.

O_{FRU} = oxygen atoms of fructose molecules; O_W = oxygen atoms of water molecules coordinated to the metal ions; av. = averaged distances.

	CaFruCl		CaFruBr		SrFruCl		SrFruBr	
	XRD	B3LYP	XRD	B3LYP	XRD	B3LYP	XRD	B3LYP
*M*1—O2	2.494 (2)	2.486	2.486 (3)	2.512	2.619 (2)	2.662	2.618 (4)	2.665
*M*1—O2*A*^{i}		2.501		2.536		2.643		2.651
*M*1—O3	2.462 (2)	2.571	2.470 (3)	2.509	2.591 (3)	2.634	2.606 (3)	2.642
*M*1—O3*A*^{i}		2.544		2.531		2.663		2.666
*M*1—O6*B*^{ii}	2.455 (2)	2.567	2.468 (3)	2.527	2.579 (2)	2.712	2.614 (3)	2.725
*M*1—O6*C*^{iii}	2.455 (2)	2.520		2.511		2.702		2.779
*M*1—O1$_W$	2.450 (2)	2.622	2.450 (3)	2.522	2.550 (4)	2.665	2.557 (4)	2.666
*M*1—O1$_W$*A*^{i}		2.502		2.681		2.679		2.679
*M*1—*X*1	5.079 (1)	4.200	5.258 (1)	4.308	5.058	4.284	5.224 (1)	4.471
*M*1—*X*1*A*^{i}		4.532		4.380		4.256		4.658
*M*1—*X*1*B*^{ii}	4.852 (1)	4.655	5.051 (1)	4.801	4.877	5.066	5.044 (1)	4.872
*M*1—*X*1*C*^{iii}		4.744		4.946		4.899		4.820
M^{2+}—O_{FRU} av.	2.470	2.532	2.475	2.521	2.596	2.669	2.613	2.688
M^{2+}—O_W av.	2.450	2.562	2.450	2.602	2.550	2.672	2.558	2.672
$M^{2+}\cdots M^{2+}$	7.839	7.450	7.888	7.876	7.941	7.741	8.024	7.738
$M^{2+}\cdots X^{-}$ av.	4.966	4.533	5.155	4.609	4.968	4.626	5.134	4.705

Symmetry codes: (i) $-x+2, y-1, -z-2$; (ii) $-x+2, y+1, -z+2$; (iii) $x, y-1, z$.

900 and 940 nm, and they were grouped per wavelength with a binning size of *ca* 6 nm. The resulting mean values are plotted together with error bars related to the standard deviation of the averages in the selected bin (Fig. 1). The wavelength range was chosen according to the filter setup range in order to reject the excitation source and measure the actual SH signal.

The SH intensities were measured sampling layers with thickness $30 < l < 100$ µm. The thickness of the sample was measured using a three-dimensional SH imaging of the sample with a *Z*-step of *ca* 5 µm. The overall *Z* scan range was chosen in accordance with the three-dimensional extension of the sample, estimating the actual thickness of the sample.

3. Results and discussion

3.1. X-ray structures

Compounds CaFruCl, CaFruBr, SrFruCl and SrFruBr are isomorphs, that is atoms that show the same disposition in the cell, crystallizing in the same space group. The cell volumes are only slightly different so these compounds can be effectively considered as isomorphs (Table 1).

The asymmetric unit of all compounds contains one fructose molecule, one half of a calcium ion, one chloride, one water molecule coordinated to the calcium ion and one half of a free water molecule. Analyzing the crystal packing, two fructose molecules bridge two metal ions, and an infinite thread of fructose and calcium ions develops in the [010] direction (Fig. 2). Consequently, these compounds have to be thought of as a uni-dimensional MOF (1D-MOF) of a special type, because the multi-dentate ligand is a neutral molecule (fructose), whereas the metal atom is +2 charged. The halogen ions and the free water molecules are inserted between the Ca-fructose threads, strictly connected through strong hydrogen bonds to the sugar molecules and to the water molecules coordinated to the metal. Those bonds contribute to stabilize the crystal. The hydrogen-bond distances and angles for all compounds are listed in the supporting information.

As can be observed from the data in Table 1, the main difference in structure among the four compounds is the cell volume, in turn influenced by the different volumes of the ions involved. Comparing the pairs CaFruCl/SrFruCl and CaFruBr/SrFruBr (different alkaline-earth metal, but same halogen anion for each pair), the expected increase in cell volume induced by the heavier atom (from Ca to Sr) is lower with respect to the corresponding increase of the pairs CaFruCl/CaFruBr and SrFruCl/SrFruBr (same metal, different halogen anion). Thus, the presence of the bromide atom implies a

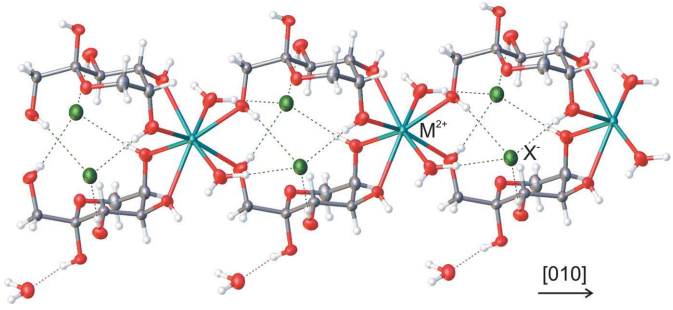

Figure 2
The infinite network of metal and halogen ions and sugar molecules for the structure of the compounds.

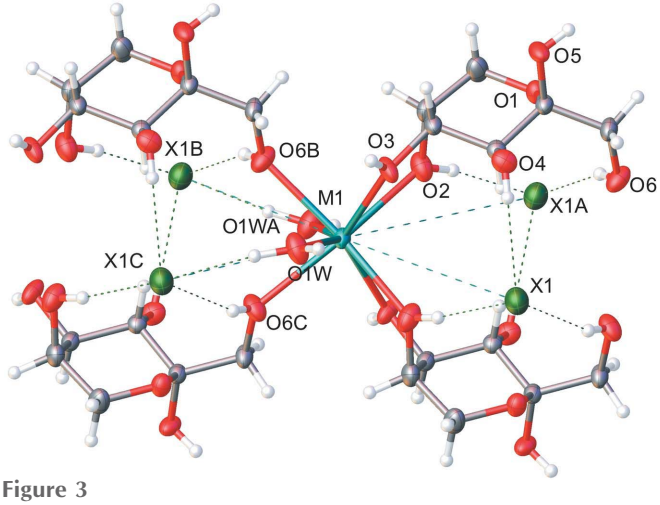

Figure 3
Coordination around the metal atom for compounds.

Table 3
Theoretically computed dipole moments μ, mean polarizabilities $\langle\alpha\rangle$, first static hyperpolarizabilities β_{tot} and second-order susceptibilities $\chi^{(2)}$.

	CaFruCl	CaFruBr	SrFruCl	SrFruBr
μ (Debye)	44.108	42.678	38.793	38.204
$\langle\alpha\rangle$ (a.u.)	691.078	741.549	680.171	728.274
β_{tot} (10^{-30} cm^5 esu^{-1})	14.6	17.9	15.5	17.9
$\chi^{(2)}$(pm V^{-1})	2.87	3.47	2.96	3.38

significant increase of cell volume with respect to the chloride, whereas the change from Ca to Sr exerts a smaller influence on the enlargement of the structure. In Fig. 3 the environment around the metal atom is shown and in Table 2 the relevant distances are reported.

Comparing the averaged values of the distances M^{2+}—O_{FRU}, M^{2+}—O_W, $M^{2+}\cdots M^{2+}$ and $M^{2+}\cdots X^-$, different trends are observed. Whereas M^{2+}—O_{FRU} and M^{2+}—O_W bonds are significantly influenced by the cation, the $M^{2+}\cdots M^{2+}$ distances increase gradually from CaFruCl to SrFruBr and this reflects in the elongation of the *b*-axis (see Table 1). In contrast, the $M^{2+}\cdots X^-$ distances are influenced mainly by the anion, mirroring the behavior of the cell volumes. In practice, we observe a gradual elongation of the metal–sugars 'thread' from CaFruCl to SrFruBr, but the transversal connections with the anions show constant distances in the pairs CaFruCl/SrFruCl and CaFruBr/SrFruBr.

3.2. Computational results

The geometries of the four complexes were obtained by optimizing the atomic coordinates from the X-ray experiments of the crystal fragments shown in Fig. 1, composed of three calcium ions, six fructose molecules, nine water molecules and six chloride ions. In Table 2 the optimized atomic distances of the complexes are compared with the corresponding values from X-ray diffraction. The reported values are in good agreement, showing small deviations, probably due to the intermolecular interactions in the crystalline state. The maximum difference between the average bond lengths M^{2+}—O_{FRU} in the four compounds is observed for SrFruBr and it does not exceed 0.075 Å. The larger deviation for the M^{2+}—O_W average bonds is not higher than 0.15 Å. Regarding the average distances $M^{2+}\cdots X^-$, the larger deviation is observed in CaFruBr between Ca^{2+} and Br^- and is 0.55 Å. However, the increase in distance from $M^{2+}\cdots Cl^-$ to $M^{2+}\cdots Br^-$, observed from X-ray diffraction, is well reproduced both for the calcium compounds and for the strontium ones.

In Table 3 the computed values of the dipole moment (μ), mean polarizability ($\langle\alpha\rangle$), first static hyperpolarizability (β_{tot}) and second-order susceptibility ($\chi^{(2)}$) are reported for all compounds. These quantities calculated at the level of calculation and with the basis set indicated in §2 are considered to be sufficiently accurate (Suponitsky *et al.*, 2008; Si & Yang, 2012) and may be safely compared even in the absence of experimental data.

The total dipole moments and the mean polarizabilities in a Cartesian frame are defined (Kanis *et al.*, 1994; Kyrill *et al.*, 2008) respectively as

$$\mu = \left(\mu_x^2 + \mu_y^2 + \mu_z^2\right)^{1/2} \quad (1)$$

and

$$\langle\alpha\rangle = (1/3)\left(\alpha_{xx} + \alpha_{yy} + \alpha_{zz}\right). \quad (2)$$

The total intrinsic hyperpolarizability β_{tot} is defined as

$$\beta_{tot} = \left(\beta_x^2 + \beta_y^2 + \beta_z^2\right)^{1/2}, \quad (3)$$

where $\beta_x = \beta_{xxx} + \beta_{xyy} + \beta_{xzz}$, $\beta_y = \beta_{yyy} + \beta_{yzz} + \beta_{yxx}$ and $\beta_z = \beta_{zzz} + \beta_{zxx} + \beta_{zyy}$.

The relationship between the macroscopic second-order susceptibility and the microscopic total hyperpolarizability is given by

$$\chi^{(2)} = NF\beta_{tot}, \quad (4)$$

where N is the number of particles *per* unit volume and F is the local field factor, assumed to be one. As F depends on crystal symmetry and the compounds studied in this work have the same structure, for all compounds the same value was attributed to F.

Table 3 shows that the values of the total dipole moment, polarizability and hyperpolarizability for these compounds are similar, with some systematic differences due to the composition of the compounds. The dipole moment is more affected by the cation, the compounds with calcium having a dipole moment greater than those with strontium. Instead, the polarizability and hyperpolarizability values are more influenced by the anion, the compounds that contain the bromine anion showing the highest values.

The calculated static susceptibility $\chi^{(2)}$ values for the compounds with the bromine anion are larger than the corresponding compound with the chloride anion (the difference in $\chi^{(2)}$ is 0.6 pm V^{-1} from CaFruCl to CaFruBr and 0.42 pm V^{-1} from SrFruCl to SrFruBr). On the other hand, a comparison of the values between compounds containing the same anion but different cations shows that different cations only slightly influence the $\chi^{(2)}$ values.

Thus, as the hyperpolarizability and static susceptibility values correlated to the SHG properties of the compounds, the theoretical calculations of these quantities suggest that compounds with the greatest and more polarizable anion should show higher SHG properties, whereas the cation does not play a significant role in determining the SHG property.

3.3. Second-harmonic generation analysis

In Fig. 3 the extracted quadratic fitting parameters of the SH intensities as a function of the excitation power at different excitation wavelengths for all the analyzed compounds are plotted.

Taking into account the variability of the measurements, Fig. 3 shows that the compounds considered in this work do not show large differences in SH intensity at all the excitation wavelengths considered. This behavior suggests that the SHG efficiency mainly depends on their structural assembly, which

is the same for all compounds. Furthermore, for the compounds containing the calcium ion the SH intensity seems on average higher at almost all the excitation wavelengths with respect to the compounds containing strontium. In particular, CaFruCl has two peaks when excited with wavelengths around 920 and 935 nm. From the chemical point of view, the measured SH intensity agrees with the calculated values of β_{tot} and $\chi^{(2)}$ which suggests similar NLO behavior for all these compounds. On the other hand, whereas the computed increase of SH intensity in the presence of Br^- instead of Cl^- is confirmed by experiments for the Sr compounds (SrFruBr with respect to SrFruCl), for the Ca compounds (CaFruCl and SrFruBr) this behavior is unclear. The experimental values refer to a global behavior of powders and can be affected by several sources of uncertainty. Consequently, caution must be exercised in comparing these compounds. Uncertainties involve optical aspects, such as local transmittance of the optical signals towards the sample or the detector, and the scattering of the emitted light through the powder itself. The use of microscope objectives ensures a limitation on the depth of field of the order of a few micrometres, even if the local thickness of the powder is not constant in all the samples. The objective focal volume reasonably confines the SH emitted intensity, due to the nonlinear optical nature of the SH process that requires a high local concentration of photons to be generated with higher probability. The variation of the powder thickness, however, could affect the transmittance of the samples and thus partially affects the comparability of the results. Due to the hygroscopic nature of some of the samples, it was not possible to obtain a constant thickness for all the samples. This fact could partially account for the differences between experimental and theoretical data in this work.

XRPD patterns, IR and Raman spectra of the powders of all compounds were collected before and after irradiation and no significant changes were detected (see the supporting information), showing that the compounds are stable.

The compounds studied in this work exhibit features that could be interesting for biomedicine applications, such as the biocompatibility due to their non-toxic components and the significant SH emission, that can permit exploitation for *in vitro* bio-imaging (Kachynski *et al.*, 2008). Thus, one would want to estimate the observed SH intensity in the operating *in vitro* conditions for SH microscopy. To this purpose assumptions have to be made, namely the absence of phase match and the smallness of crystal size with respect to the coherence length. Under these assumptions, the model of Perry (Kurtz & Perry, 1968) predicts the intensity of the SH to be linearly dependent of the thickness l of the layer of nanoparticles. In our experiments the SH intensities were obtained sampling layers with thickness $30 < l < 100$ µm, as reported in §2. The thickness of stacks of MnO nanoparticles of average size 11 nm inside HeLa cells can be estimated using the work of Costanzo (Costanzo *et al.*, 2016) to be $l' = 2$ µm. For the same thickness, the model of Kurtz & Perry (1968) would predict the SH intensity of β-D-fructopyranose alkaline halides nanoparticles to be lowered by a factor of $0.02 < l'/l < 0.07$ with respect to the intensity used to obtain the quadratic coefficients, and we anticipate the resulting SH intensity to be detectable by an NLO multimodal microscope.

4. Conclusions

In this work, we had the unusual possibility of being able to analyze four fructose-salt compounds sharing the same structure with different combinations of Ca/Sr and Cl/Br ions. Theoretical calculations suggested that the SH efficiency is much influenced by the anion, the first static hyperpolarizability and second-order susceptibility being higher for bromide compounds with respect to those with chloride. In contrast, the cation does not seem to play a significant role in the SHG properties. The structure analysis showed that the compounds containing bromide show a significant difference in the cell volumes with respect to the compounds with chlorine, mainly due to longer cation–anion distances. These results confirm that both the intrinsic nature of the anion and the induced dissociation of $M\cdots X$ by fructose play a role in the SHG properties of such compounds, as suggested in our previous work (Marabello *et al.*, 2015).

Experimental SHG measurements of SH intensity on these compounds have similar values, taking in to account experimental errors. This similarity was expected since they share the same structure. However, the relative SH intensities remain unexplained, due to both uncertainty in measurements and the difficulties caused by the hygroscopic behavior of these compounds. Finally, we estimated the SH intensity in the operative biological environment and one would expect that these compounds should be suitable for biological applications.

References

Agilent (2014). *CrysAlisPro*, Version 1.171.37.31 (release 14-01-2014 CrysAlis171. NET, compiled Jan 14 2014, 18:38:05). Agilent Technologies, Yarnton, England.

Agullo-Lopez, F., Cabrera, J. M. & Agullo-Rueda, F. (1994). *Electrooptics: Phenomena, Materials and Applications*. New York: Academic Press.

Bäumner, R., Bonacina, L., Enderlein, J., Extermann, J., Fricke-Begemann, T., Marowsky, G. & Wolf, J.-P. (2010). *Opt. Express*, **18**, 23218–23225.

Becke, A. D. (1988). *Phys. Rev. A*, **38**, 3098–3100.

Becke, A. D. (1993). *J. Chem. Phys.* **98**, 5648–5652.

Bourhill, G., Mansour, K., Perry, K. J., Khundkar, L., Sleva, E. T., Kern, R., Perry, J. W., Williams, I. D. & Kurtz, S. K. (1993). *Chem. Mater.* **5**, 802–808.

Chandrasekaran, J., Ilayabarathi, P., Maadeswaran, P., Kutty, P. M. & Pari, S. (2012). *Opt. Commun.* **285**, 2096–2100.

Cook, W. J. & Bugg, C. E. (1976). *Acta Cryst.* B**32**, 656–659.

Costanzo, M., Scolaro, L., Berlier, G., Marengo, A., Grecchi, S., Zancanaro, C., Malatesta, M. & Arpicco, S. (2016). *Int. J. Pharm.* **508**, 83–91.

Craig, D. C., Stephenson, N. C. & Stevens, J. D. (1974*a*). *Cryst. Struct. Commun.* **3**, 195–199.

Craig, D. C., Stephenson, N. C. & Stevens, J. D. (1974*b*). *Cryst. Struct. Commun.* **3**, 277–281.

Dempsey, W. P., Fraser, S. E. & Pantazis, P. (2012). *Bioessays*, **34**, 351–360.

Dhanuskodi, S., Vasantha, K. & Mary, P. A. A. (2007). *Spectrochim. Acta A Mol. Biomol. Spectrosc.* **66**, 637–642.
Dolomanov, O. V., Bourhis, L. J., Gildea, R. J., Howard, J. A. K. & Puschmann, H. (2009). *J. Appl. Cryst.* **42**, 339–341.
Frisch, M. J. *et al.* (2009). *GAUSSIAN*09, Revision, A.02, Gaussian, Inc., Wallingford, CT, USA.
Guo, J. & Zhang, X. (2004). *Carbohydr. Res.* **339**, 1421–1426.
Haber, L. H., Kwok, S. J. J., Semeraro, M. & Eisenthal, K. B. (2011). *Chem. Phys. Lett.* **507**, 11–14.
Hehre, W. J., Radom, L., Schleyer, P. v. R. & Pople, J. A. (1986). *Ab Initio Molecular Orbital Theory*. New York: Wiley.
Jiang, M. & Fang, Q. (1999). *Adv. Mater.* **11**, 1147–1151.
Kachynski, A. V., Kuzmin, N., Nyk, M., Roy, I. & Prasad, P. N. (2008). *J. Phys. Chem. C*, **112**, 10721–10724.
Kanis, D. R., Ratner, M. A. & Marks, T. J. (1994). *Chem. Rev.* **94**, 195–242.
Kannan, S., Goetz-Neunhoeffer, F., Neubauer, J., Pina, S., Torres, P. M. C. & Ferreira, J. M. F. (2010). *Acta Biomater.* **6**, 571–576.
Kuppler, R. J., Timmons, D. J., Fang, Q.-R., Li, J.-R., Makal, T. A., Young, M. D., Yuan, D., Zhao, D., Zhuang, W. & Zhou, H.-C. (2009). *Coord. Chem. Rev.* **253**, 3042–3066.
Kurtz, S. K. & Perry, T. T. (1968). *J. Appl. Phys.* **39**, 3798–3813.
Kyrill, Y., Suponitsky, K. Y., Tafur, S. & Masunov, A. E. J. (2008). *Chem. Phys.* **129**, 044109.1–044109.11.
Marabello, D., Antoniotti, P., Benzi, P., Canepa, C., Diana, E., Operti, L., Mortati, L. & Sassi, M. P. (2015). *J. Mater. Sci.* **50**, 4330–4341.
McKinlay, A. C., Morris, R. E., Horcajada, P., Férey, G., Gref, R., Couvreur, P. & Serre, C. (2010). *Angew. Chem. Int. Ed.* **49**, 6260–6266.
Mortati, L., Divieto, C. & Sassi, M. P. (2012). *J. Raman Spectrosc.* **43**, 675–680.
Pantazis, P., Maloney, J., Wu, D. & Fraser, S. E. (2010). *Proc. Natl Acad. Sci.* **107**, 14535–14540.
Parsons, D. F. & Ninham, B. W. (2009). *J. Phys. Chem. A*, **113**, 1141–1150.
Schlegel, H. B. (1982*a*). *J. Chem. Phys.* **77**, 3676–3681.
Schlegel, H. B. (1982*b*). *J. Comput. Chem.* **3**, 214–218.
Schlegel, H. B., Binkley, J. S. & Pople, J. A. (1984). *J. Chem. Phys.* **80**, 1976–1981.
Schlegel, H. B. & Daudel, C. (1981). *Computational Theoretical Organic Chemistry*. Dordrecht: Reidel Publishing Co.
Sheldrick, G. M. (2015*a*). *Acta Cryst.* A**71**, 3–8.
Sheldrick, G. M. (2015*b*). *Acta Cryst.* C**71**, 3–8.
Si, Y. & Yang, G. (2012). *Mol. Phys.* **110**, 333–341.
Staedler, D. *et al.* (2012). *ACS Nano*, **6**, 2542–2549.
Suponitsky, K. Y., Tafur, S. & Masunov, E. (2008). *J. Chem. Phys.* **129**, 044109, 1–11.
Tam, W., Guerin, B., Calabrese, J. C. & Stevenson, S. H. (1989). *Chem. Phys. Lett.* **154**, 93–96.
Wunderlich, S. & Peschel, U. (2013). *Opt. Express*, **21**, 18611–18623.